# COMPLIANT MICROGRIPPER WITH PARALLEL STRAIGHT-LINE JAW TRAJECTORY FOR NANOSTRUCTURE MANIPULATION

**Justin Beroz, Shorya Awtar, Mostafa Bedewy, Sameh Tawfick, and A. John Hart**
**Department of Mechanical Engineering**
**University of Michigan**
**Ann Arbor, MI, USA**

## INTRODUCTION

Compliant gripping mechanisms are particularly suited for precision manipulation of micro- and nanoscale objects by virtue of having zero backlash, no parasitic columbic friction effects, and often only requiring one actuator to close two gripping faces symmetrically about a centerline of action. Many previous compliant gripping mechanisms use a parallelogram structure (Fig. 1a) to close parallel jaws [1,2,3]. These designs are effective in gripping micron-sized objects, but the gripping faces inherently move along an arc-shaped trajectory (Fig.1b). Straight-line jaw motion may be desired for micromechanical tension/compression tests, and for gripping soft objects such as cells, gels, and assemblies of nanostructures such as carbon nanotubes. These and other applications are sensitive to normal and shear loading. In general, the transverse component of the jaw motion constitutes a coupling of two sources of transverse error (δ) in the mechanism: *kinematic error,* defined as the motion path of an equivalent rigid link model, and *elastic error* stemming from finite material elasticity.

We present a compliant gripping mechanism (Fig. 1c) that exhibits a straight-line parallel jaw trajectory. The input (tab) and output (gripper jaw) displacements are proportional, and the proportionality factor can be varied by design. This gripper is a lumped-compliance based flexure mechanism developed from an analogous rigid-link-and-pin-joint mechanism (Fig. 1d). Transverse errors (δ), stemming primarily from linear-elastic structural compliance, are corrected by modifying the mechanism geometry to incorporate kinematic compensation trajectories that redress these errors by superposition. The resulting compliant microgripper features zero *kinematic error,* and the *elastic error to jaw stroke ratio* (δ/d) is minimized to $2.5 \times 10^{-5}$. By comparison, a parallelogram configuration of equivalent beam dimensions has a ratio of $4.35 \times 10^{-3}$. Further, a parallelogram gripper would require beam lengths at least one order of magnitude larger than the dimensions of our proposed design to achieve a similar straightness in output path over the same jaw range.

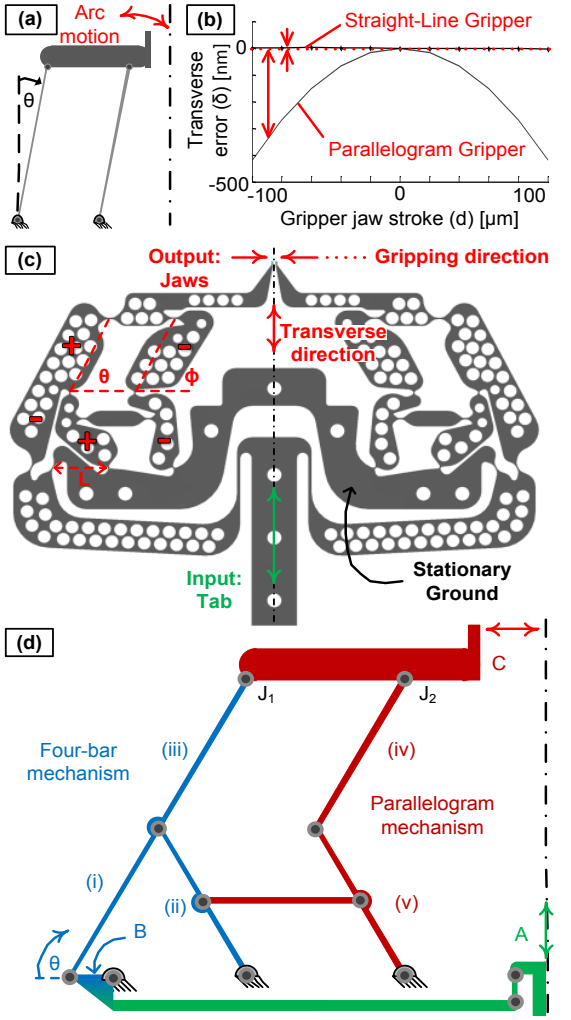


*FIGURE 1. (a) Rigid link kinematic model of a typical parallelogram mechanism gripper, (b) comparison of output paths between our straight-line gripper (solid) and a parallelogram (dashed) having equivalent beam dimensions, (c) our straight-line compliant gripper based on an analogous kinematic model shown in (d). (note: mechanisms are symmetric about the centerlines shown).*

## KINEMATIC DESIGN

The proposed design was conceived as a rigid-link-and-pin-joint mechanism (Fig 1d) comprising 3 parts: a four-bar mechanism that defines the location of $J_1$ in terms of link B angle (blue); a mechanism that translates the vertical linear motion of the input tab, A, into rotation of link B (green); and a parallelogram-based mechanism that replicates the motion path of $J_1$ at $J_2$, which enables translation of the gripper face, link C, without rotation (red). The four-bar mechanism is a version of the classic "Hoekens" linkage [4] which we optimized for straightness of output path (Fig.2). A notable feature of this linkage is that the angular displacement of link B is approximately linearly related to the translational displacement of $J_1$ over the stroke range. Further, the maximum displacement of the input tab changes the angle of link B by less than two degrees, which linearly relates input tab and gripper jaw displacements by means of small angle approximation.

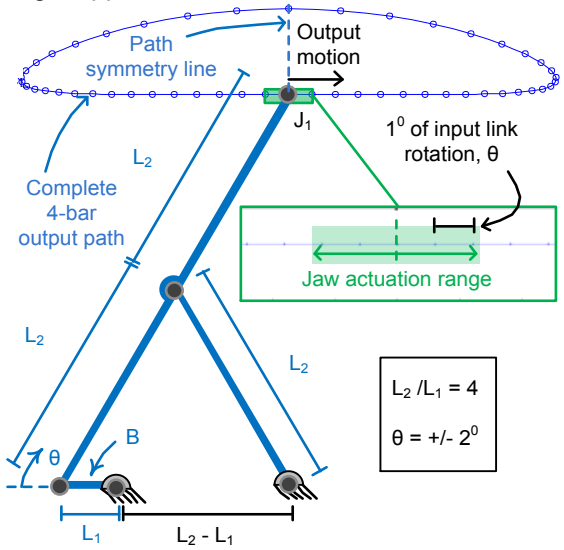


*FIGURE 2. Four-bar motion characteristics and beam length relations for optimization*

We determined two important relationships between the beam lengths of the four-bar linkage: (1) symmetry of the output path is maintained by relating link lengths $L_1$ and $L_2$ as shown in Fig. 2; and (2) the ratio $L_2/L_1$ determines the curvature of the output path. We wrote a kinematic linkage solver program in MATLAB that iteratively converged upon the ratio $L_2/L_1$=4, for the straightest output trajectory along the bottom portion of the output path. This output path is still an *approximate* straight line in a strict mathematical sense; there is a slight concave-upwards curvature along this bottom portion. But, this deviation (δ/d) is $5x10^{-11}$ over the prescribed range of jaw actuation. In terms of the actual gripper dimensions ($L_1$= 5/3 mm, $L_2$= 6+2/3 mm), this kinematic error (δ) is 0.01 pm, which is negligible considering fabrication tolerances.

## LUMPED-COMPLIANCE MECHANISM

This rigid-link-and-pin-joint mechanism was then translated into a lumped-compliance flexure mechanism (Fig. 1c). Thin compliant hinges occupy points of rotation between significantly wider sections that approximate the rigid links. The hinges have a cycloidal profile [5] which, compared to other compliant hinge contours, maximizes in-plane rotational compliance and translational stiffness for a prescribed angular deflection and material strain limit. Limits of angular deflection ($<2^0$) and allowable material strain (<0.5% for Si) were established for our design.

## JAW MOTION OPTIMIZATION

Actuation of the gripper was simulated by two-dimensional non-linear finite element analysis (FEA) using ANSYS. FEA simulations revealed an error ratio (δ/d) of $5x10^{-3}$ at the gripper jaws. Translational error of the gripper jaw is caused by errors in the trajectory of $J_1$. Jaw rotation is attributable to inaccurate replication of $J_1$ motion at $J_2$. These errors may be attributed to two general elastic effects: deflections in the large area geometries, which invalidate the rigid link approximation; and drifts in the rotational centers of the compliant hinges, which invalidate the pin joint approximation.

### Elastic error characterization

In our lumped compliance mechanism, stresses develop due to moments exerted by the flexure hinges under bending. To characterize these stresses, we created an analytical model of the four-bar and parallelogram mechanism, using rigid links connected by torsional spring pin joints. We calculated the forces and moments acting at each joint when link B (Fig. 1d) is rotated by a small angle. Using this model, we can understand the development of stresses in the mechanism, which manifest the elastic errors. We determined that, when the gripper is actuated so as to close the jaws, (i.e. downward displacement of the input tab and clockwise rotation of link B), tensile stress develops in the links marked '+' and compressive stress develops in the links marked '-' (Fig. 1c). Since these links and flexure hinges have finite elastic

stiffness, this stress development produces two distinct linear-elastic effects, which we call *parallelogram coupling* and *four-bar loading*.

The tensile stresses in links (ii) and (iii), and compressive stresses in links (iv) and (v) (Fig. 1c,d), constitute a differential loading which, due to material elasticity, produces a 1st order clockwise rotation of the gripping link over this closing jaw stroke as illustrated by the asterisks (*) in Fig.3a. It is analogous to linear elastic effects in a parallelogram flexure, which have been well characterized and described by closed form equations [6]. Moreover, the tension in links (ii) and (iii) effectuate a 1st order error component in the $J_1$ trajectory, as shown by the asterisks in Fig. 3b. We call this effect a linear-elastic motion due to *parallelogram coupling*.

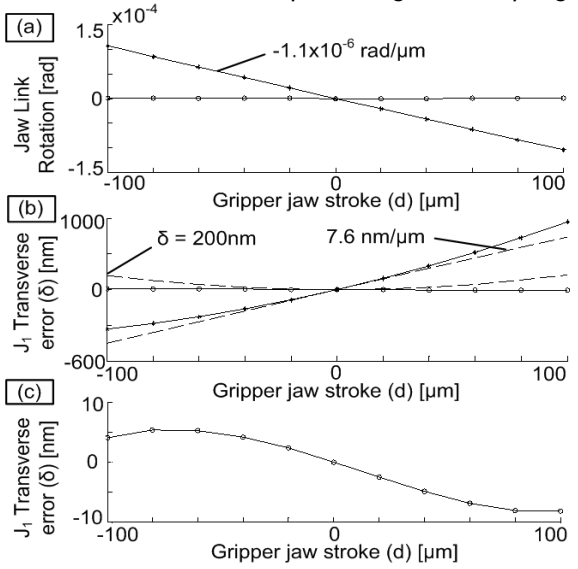


*FIGURE 3. (a) Jaw link rotation over stroke for initial (*) and optimized (o) FE simulations; (b) $J_1$ trajectory over jaw stroke for initial (*) and optimized (o) FE simulations, initial trajectory is also shown decomposed into its 1st and 2nd order components (--).*

Compression in link (i) and tension in link (ii) (Fig. 1c,d) generate a 2nd order error component in the trajectory of $J_1$. We modeled this effect by modifying the MATLAB linkage program to linearly lengthen or shorten the link length during the stroke to simulate compliance. Using this model, we isolated the error contribution for each link, and determined that compliance in links (i) and (ii) can independently create this 2nd order error, and the combination of these contributions is additive. We call this effect a linear-elastic motion due to *four-bar loading*.

Since the compliance in the mechanism is predominantly linear-elastic, we may use the principle of superposition to deconstruct the observed error motion characteristics. Thus, we can isolate the contributions of parallelogram coupling and four-bar loading at $J_1$ by subtracting a linear fit from the trajectory curve, as illustrated by the dashed lines in Fig. 3b.

**Geometric Correction**

There are three error motions that must be counteracted to correct the gripper jaw trajectory: 1st order error at $J_1$, 2nd order error at $J_1$, and rotation of the gripper link. We modified the linkage geometry to adjust the mechanism's kinematic motion such that linear-elastic errors are cancelled by principle of superposition. Accordingly, these kinematic compensation trajectories are the x-axis reflection of the error motions calculated by the initial FEA simulation (Fig. 3a,b: asterisks), i.e., producing a $J_1$ 1st order trajectory of -7.6 nm/μm, $J_1$ 2nd order trajectory of -200 μm deviation at full stroke, and rotation of $1.1\text{x}10^{-6}$ rad/μm. Consequently, we define and perturb three geometric parameters (Fig. 1c): θ, which changes the 1st order trajectory of $J_1$; L, which counteracts the 2nd order motion of $J_1$; and Φ, which counteracts the gripper jaw rotation by introducing a non-parallel angular offset between links (iii) and (iv).

The kinematic model predicts the following modifications to correct the jaw trajectory: $\Delta\theta_{KE} = -0.880^0$, $\Delta L_{KE} = -0.7$ mm and $\Delta\Phi_{KE} = -0.386^0$. These predictions differ less than 10% from the optimal correction factors determined by iterative geometric modification of the FEA model: $\Delta\theta_{FE} = -0.850^0$, $\Delta L_{FE} = -0.7$ mm and $\Delta\Phi_{FE} = -0.354^0$. Residual $J_1$ translational (δ/d) and jaw rotation errors of the optimized mechanism, according to FEA simulation, are $4\text{x}10^{-5}$ and 0.8 μrad respectively. Due to the small magnitude and highly non-linear path of this error (Fig. 3c), it may be attributable to elasto-kinematic effects.

**FABRICATION AND TESTING**

We are working to fabricate a prototype microgripper from a (111) silicon wafer (4" diameter, 500 μm thick) using a through-wafer Deep Reactive Ion Etching (DRIE) process. We chose this crystallographic orientation because silicon has a uniform modulus of elasticity in any direction coplanar with the (111) crystal plane. Therefore, the wafer can be treated as an isotropic material for our case of in-plane bending.

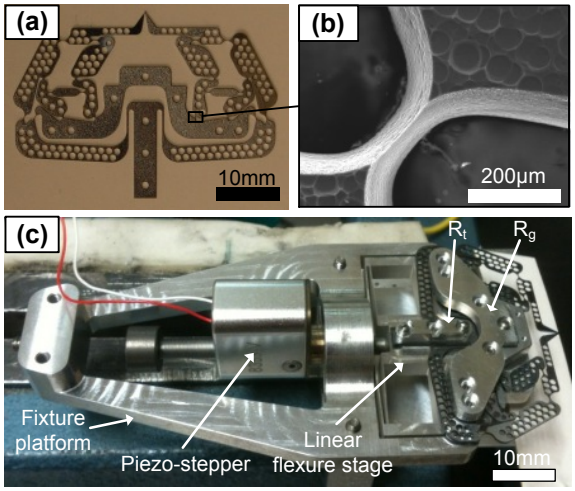


*FIGURE 4. (a) Prototype microgripper etched from a (100) silicon wafer, (b) SEM image of joint, showing sidewall due to improper etch recipe, (c) test fixture with piezo actuator and integrated linear flexure stage.*

We designed a mask pattern that fits four grippers on one wafer, with each gripper measuring approximately 40 mm by 28 mm. With these dimensions, the jaw range (d) and error (δ) are predicted to be 400 μm and 2.5 nm, respectively. For comparison, a parallelogram gripper would require beams greater than one half meter in length to achieve a similar straightness in output path over this jaw range.

The DRIE process generates heat which scales with the size of etch area. Because etch rates are highly sensitive to temperature, thermal variations across the wafer cause non-uniform etching of the gripper pattern. Consequently, we designed the lithography mask pattern such that only a 50 μm wide kerf line is etched around all of the gripper geometry. We fabricated our first prototypes (Fig. 4a) using an etch recipe that resulted in 2.2 μm scalloping and 10 μm/minute etching rate with a selectivity ≈70:1. However, dimensional accuracy of these microgrippers is poor due to significant tapering of the side walls (Fig. 4b). We are working to optimize our mask patterning technique and etch recipe to achieve nearly vertical side walls with minimal scalloping.

Nonetheless, we have mounted the non-uniformly etched gripper on our custom fixture (Fig. 4c) and actuated the jaws fully closed without breakage. The gripper is secured along the ground link by the top retaining piece ($R_g$), which is fastened by screws threaded into the fixture platform. The gripper tab is constrained to move linearly and in-plane by a double-parallelogram flexure stage in the fixture platform. The flexure stage was made by wire EDM. The input tab is fastened to this linear stage by the top retaining piece ($R_t$). The stage is pre-loaded against, and actuated by, a piezo-stepper with <30 nm step size. We expect this to correspond to <6 nm incremental motion of the gripper jaws. We designed the entire fixture to fit inside a Scanning Electron Microscope (SEM). Once we manufacture a dimensionally accurate compliant gripper, we will actuate the gripper jaws inside the SEM, and compute the gripper jaw trajectory and incremental step resolution via image analysis.

Because silicon is an extremely brittle material, small defects in the crystal lattice and stress concentrations from rough surfaces can reduce the fracture strain limit from the theoretical value of 4% to <0.2% [7]. Therefore, the actual achievable strain limit is largely based on the quality of the wafer and the etching process. By achieving full closure of the gripper jaws, we have shown that the DRIE-etched walls are smooth enough for our target jaw range of 0-400μm to be realized.

## REFERENCES

[1] Goldfarb M, Celanovic N. A flexure-based gripper for small-scale manipulation. Robotica. 1999; 17: 181-187.

[2] Nah S, Zhong Z. A microgripper using piezoelectric actuation for micro-object manipulation. Sensors Actuators A. 2007; 133: 218-224.

[3] Zubir M, Shirinzadeh B. Development of a high precision flexure-based microgripper. Precis Eng. 2009; 33: 362-370.

[4] DeJonge A. E. R, The Correlation of Hinged Four-Bar Straight Line Motion Devices by Means of the Roberts Theorem and a New Proof of the Latter. Ann NY Acad Sci. 1960; 84: 75-145.

[5] Tian Y, et. al. Three Flexure Hinges for compliant mechanism designs based on dimensionless graph analysis. Precis Eng. 2010; 34: 92-100.

[6] Awtar S, Slocum A. Characteristics of Beam-Based Flexure Modules. J. of Mech. Des. 2007; 129: 625-639.

[7] Ando T, et. Al. Orientation-dependent fracture strain in single-crystal silicon beams under uniaxial tensile conditions, Int. Symp. on Micro-Mechatronics and Human Science. 1997; 55-60.